Supplementary Information for:

Decline in Iceland-Scotland overflow strength over the last 7000 years

David J.R. Thornalley[1*], Michael Blaschek[2], Frazer J. Davies[2], Summer Praetorius[3], Delia W. Oppo[1], Jerry F. McManus[4], Ian R. Hall[5], Helga (Kikki) Kleiven[6], Hans Renssen[2] & I. Nicholas McCave[7].

[1] Department of Geology and Geophysics, Woods Hole Oceanographic Institution, Woods Hole, MA 02543, USA

[2] Department of Earth Sciences, Faculty of Earth and Life Sciences, VU University Amsterdam, NL-1081HV Amsterdam, The Netherlands

[3] College of Oceanic and Atmospheric Sciences, Oregon State University, Corvallis, OR 97331-5503, USA

[4] Lamont-Doherty Earth Observatory, Earth Institute at Columbia University, Palisades, New York, USA

[5] School of Earth and Ocean Sciences, Cardiff University, Cardiff, UK.

[6] Department of Earth Science, University of Bergen, Allegaten 41, N-5007 Bergen, Norway

[7] Department of Earth Sciences, University of Cambridge, Cambridge, UK.

*Correspondence to: d.thornalley@cantab.net

This pdf file includes:

Supplementary methods

Table S1-3

Figure S1-9

References

Figure S1. Plot showing the average grain size trends for each depth interval obtained using 1000-year bins, with ±2SE. The solid black and dashed grey lines for each plot are obtained by using 1000-year bins offset from one another by 500 years, demonstrating that the overall trend for each group is not strongly dependant on the precise binning interval chosen.

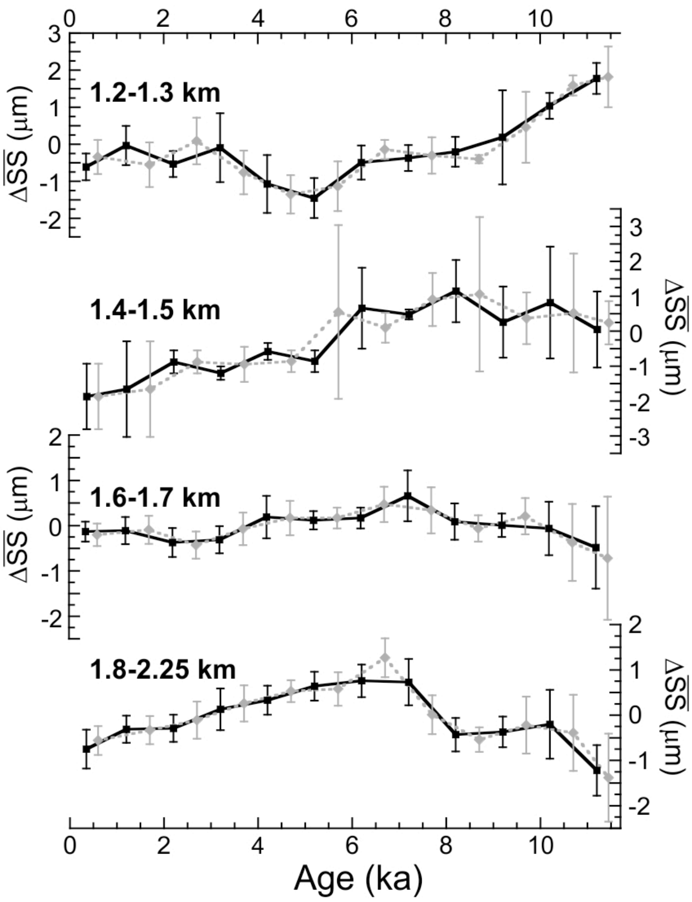

Figure S2. Comparison of the I-S overflow strength 'stack' calculated by averaging changes in the 'raw' $\overline{SS}$ versus normalized data.

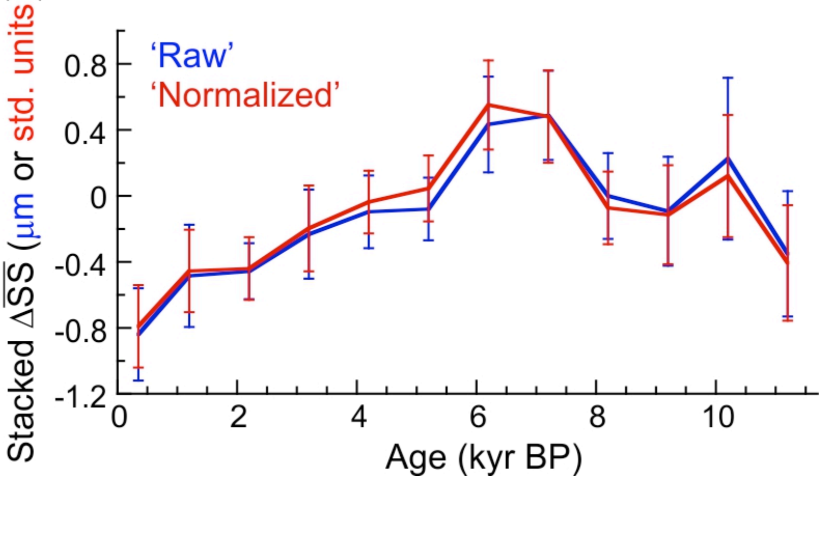

Model Description

All simulations were performed using LOVECLIM version 1.2, a global, 3-dimensional model of intermediate complexity (Goosse *et al.*, 2010). It consists of an atmosphere, ocean, sea-ice, ice-sheet, carbon cycle, iceberg, land and vegetation components, of which, the atmosphere, ocean, sea-ice, land and vegetation components were utilised in these simulations. The applied model is an updated version of the ECBilt-CLIO-VECODE model utilized previously by Renssen *et al.* (2009) to study long-term Holocene climate change.

The atmospheric component, ECBilt, is a quasi-geostrophic model, with a spectral T21 truncation with three vertical layers at 800hPa, 500hPa and 200hPa (Haarsma *et al.*, 1996; Opsteegh *et al.*, 1998). It also contains a full hydrological cycle, in which all the atmosphere is dry above 500hPa and any moisture above this level is converted to precipitation. Clouds are prescribed in the model based on observations (Rossow *et al.* 1996). The land surface component of the model is part of ECBilt and has the same grid size. In this component river runoff is calculated as a function of vegetation, using a simple bucket method approach, in that if after precipitation, evaporation and snow melting there is additional moisture remaining, this is then added to the river mouth of the appropriate basin.

The ocean component, CLIO, consists of a free-surface general ocean circulation model (Goosse *et al.*, 1997, Deleersnijder and Campin, 1995; Deleersnijder *et al.*, 1997) coupled to a thermodynamic-dynamic sea-ice model (Fichefet and Morales Maqueda, 1997 and 1999). CLIO has a resolution of 3° in both the longitude and latitude, 20 vertical layers, realistic bathymetry and contains some classical approximations (Boussineq, thin shell and hydrostatic). The ocean model incorporates a formulation of boundary layer mixing based on the level-2.5 turbulence closure scheme of Mellor and Yamada (1982) and a parameterization of density-driven downslope flow (Campin and Goosse, 1999). It also includes isopycnal diffusion and Gent and McWilliams′ parameterization to represent meso-scale eddies in the ocean (Gent and McWilliams, 1990). The growth and decay of sea-ice in the model are represented by a three-layer model that similates an Arctic sea-ice distribution that is in general agreement with observations (Goosse *et al.*, 2010). In that snow accumulates upon a slab of ice that comprises two of the three layers. When the surface temperature drops below the melting point, snow is able to accumulate. Upon sufficient accumulation of snow, the slab becomes submerged below the surface of the water, which coupled with freezing seawater, increases the thickness of the ice (Fichefet and Morales Maqueda, 1997).

The vegetation component, VECODE, is a reduced-form dynamic global vegetation model that simulates the cover of trees and grasslands, as well as deserts as a dummy type (Brovkin *et al.*, 2002). The coupling to ECBilt is through the surface albedo (Goosse *et al.*, 2010).

The climate sensitivity of LOVECLIM, to a doubling of the atmospheric CO_2, is at the lower end of the range found in global climate models with a 1.9K increase in mean global temperature after 1000 years (Goosse *et al.*, 2010). The simulated deep ocean circulation in LOVECLIM compares reasonably well with other model results (Schmittner *et al.*, 2005), with deep convection taking place in both the Labrador and Nordic Seas (Goosse *et al.*, 2010). The model has been applied successfully in different palaeoclimatological modelling studies for settings like the Last Glacial Maximum (Roche *et al.*, 2007), the 8.2 ka BP event (Wiersma and Renssen, 2006), the Holocene (Renssen *et al.*, 2009), and the Last Millennium (Goosse *et al.*, 2005).

For further information regarding model design and performance over a number of temporal and spatial scales the reader is directed to Goosse *et al*. (2010).

Experimental Design

Holocene

In this study we discuss the results of four newly performed transient Holocene experiments that cover the last 9000 years. The simulations were started at 9 ka BP because before that time the influence of the Younger Dryas cold period may still have an important influence on the climate through the long-term memory of the deep ocean. We forced all the simulations with orbital and greenhouse-gas concentrations in line with the PMIP3 protocol (http://pmip3.lsce.ipsl.fr/). An overview of the forcings is provided in Figure S1 and a summary of experiment setups in Table S1.

We performed one transient reference simulation (ORB+GHG) including only transient orbital and greenhouse gases and two transient simulations including additionally either LIS melt water (ORB+GHG+LIS(MELT)) or the full LIS forcing (ORB+GHG+LIS(MELT+ICE)). The LIS impact in the latter two experiments is prescribed following Renssen *et al*. (2009). We separately investigate the effect of an additional freshwater flux (denoted by MELT), representing the background melting of the LIS introduced at the St. Lawrence River outlet and Hudson Bay outlet, and the total effect of the remnant LIS (i.e. additional freshwater, albedo and topography changes) indicated by the name MELT+ICE. In agreement with palaeoceanographic evidence (Hillaire-Marcel *et al*., 2001 and 2007), Labrador Sea deep convection was suppressed by the LIS background melt flux.The background LIS melt flux was set to 0.09 Sv between 9 to 8.4 ka BP, decreasing slightly to 0.08 Sv between 8.4 and 7.8 ka BP, dropping to 0.01 Sv between 7.8 and 6.8 ka BP (Figure S1). These freshwater rates are based on adapted estimates by Licciardi *et al*. (1999). In ORB+GHG+LIS(MELT+ICE) the effect of the disintegrating LIS was accounted for by changing the surface albedo and the topography at 50-year time steps, interpolated from the reconstructions provided by Peltier (2004), during the period 9 to 7 ka BP.

Finally, we performed a fourth transient experiment ORB+GHG+LIS(MELT+ICE)+GIS(MELT) that included the GIS melt water flux, in addition to all forcings prescribed in ORB+GHG+LIS(MELT+ICE). This melt flux is derived from ice thickness changes provided at 500-year time steps by Peltier (2004) ICE-5G model. We have added this melt water to the top layer of the ocean corresponding to the surface runoff outlets of the Greenland landmass. As shown in Figure S1, the additional melt water was set to 13 mSv for 9 ka BP and increases to 23 mSv from 9 to 8 ka BP and then rapidly decreases to 3 mSv before vanishing completely at 7 ka BP. Possible GIS topography changes in the model are fairly small in the model grid resolution (T21) and will be neglected. Despite the imperfections in our reconstruction of the Holocene GIS changes, we argue that it provides an appropriate first-order forcing at the scale of our model.

Future Simulations

Three transient simulations covering 1850-2100AD were performed. For the period prior to 2000AD all simulations were forced with annually varying orbital parameters (Berger, 1978), total solar irradiance (Wang *et al*., 2005; Delaygue and Bard, 2009), volcanic forcings (Sato *et al*., 1993; Pinto *et al*., 1998; Crowley *et al*., 2008; Timmreck *et al*., 2009), ozone (IPCC, 2007), sulphates (IPCC, 2007) and GHG concentrations (PMIP3). For the 21st century all simulations following the SRES

A1B, A2 and B1 scenarios of the IPCC (2000), in that all forcings remained transient, except for volcanic forcing which was held constant at 2001 levels, and total solar irradiance which was held at the solar constant of LOVECLIM, 1365Wm^{-2}. These simulations were initiated from a Pre-Industrial (PI) control simulation with appropriate forcings for 1750 AD that had reached a quasi-equilibrium state. These three scenarios were chosen because they cover the full range of anthropogenic radiative forcing provided by the IPCC for the 21st Century, allowing for a wider perspective of future projections to be determined. In addition, these SRES scenarios are commonly taken in other studies, allowing for comparison. It should be noted that enhanced melt of the GIS was not included in the model simulations and the effect of this on the AMOC is expected to be small over the next century (Driesschaert *et al.*, 2007).

Table S1. Summary of model experiments

Experiment Name	Initial Conditions		GIS Melt flux [Sv]	LIS Melt flux [Sv]
ORB+GHG	Transient Orbital and Greenhouse Gases (9-0 ka BP) from PMIP3 transient simulation setup		0	0
ORB+GHG +LIS (MELT)	ORB+GHG	+ LIS melt water	0	0.09
ORB+GHG +LIS(MELT+ICE)	ORB+GHG +LIS (MELT)	+ LIS (Albedo + Topography)	0	0 - 0.09
ORB+GHG +LIS(MELT+ICE) +GIS(MELT)	ORB+GHG +LIS(MELT+ICE	+ GIS melt water	0 - 0.026	0 - 0.09

Figure S2. Transient forcing summary

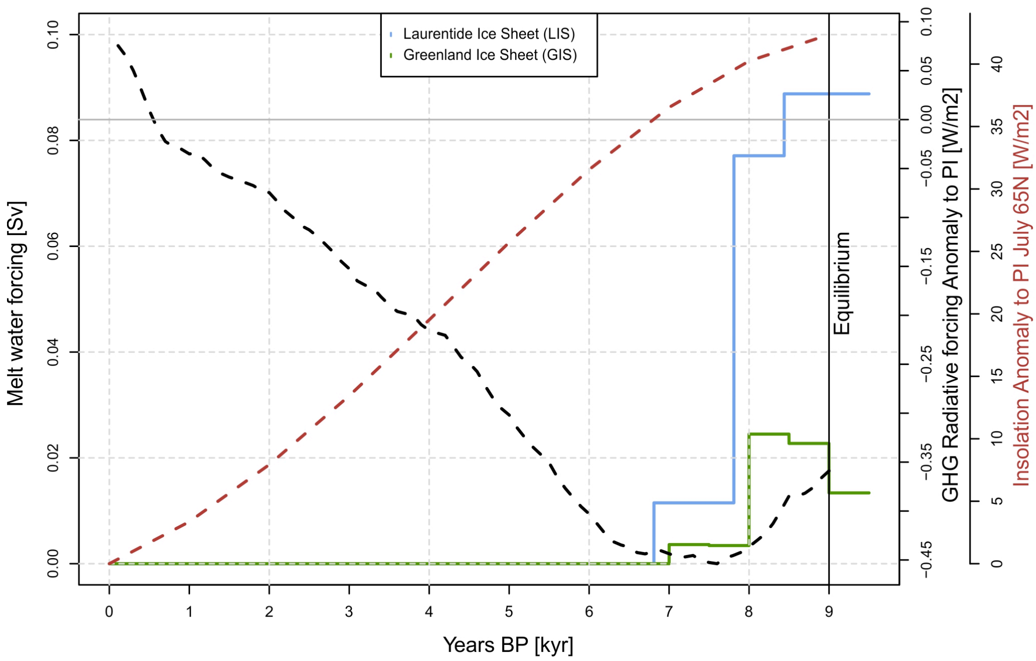

Figure S3.
500-year mean March sea surface temperature (SST) in the model convection region (15-20°E, 76.25-78.75°N) in the Nordic Seas for the Holocene transient model simulations.

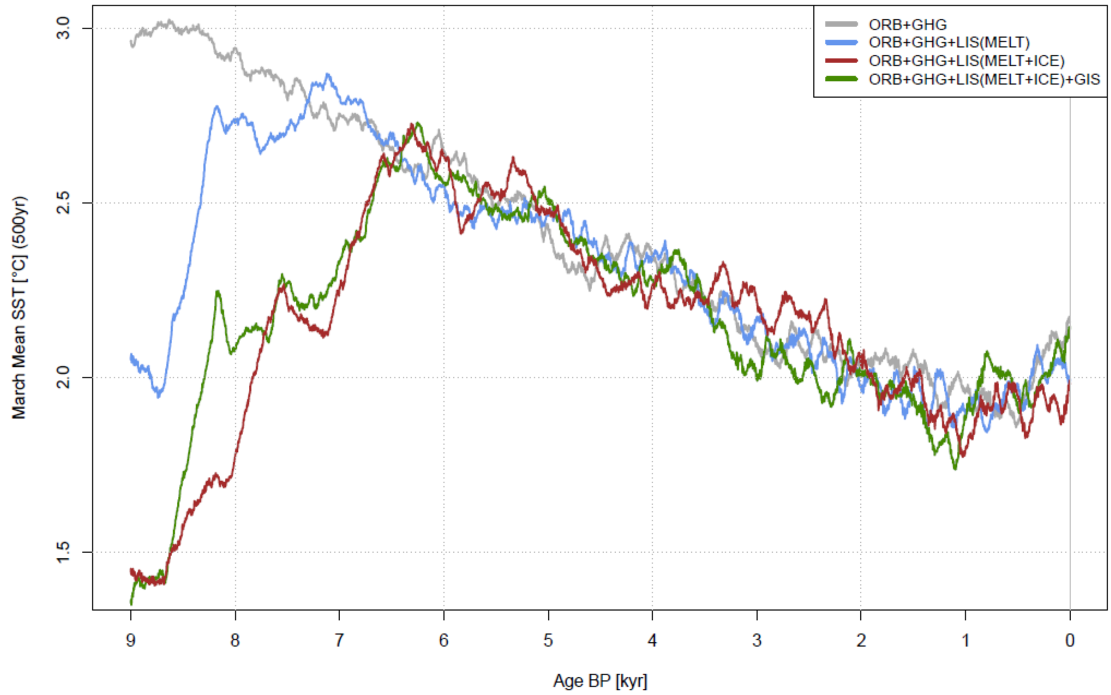

Figure S4.
500-year mean March precipitation-evaporation balance in the model convection region in the Nordic Seas for the Holocene transient model simulations.

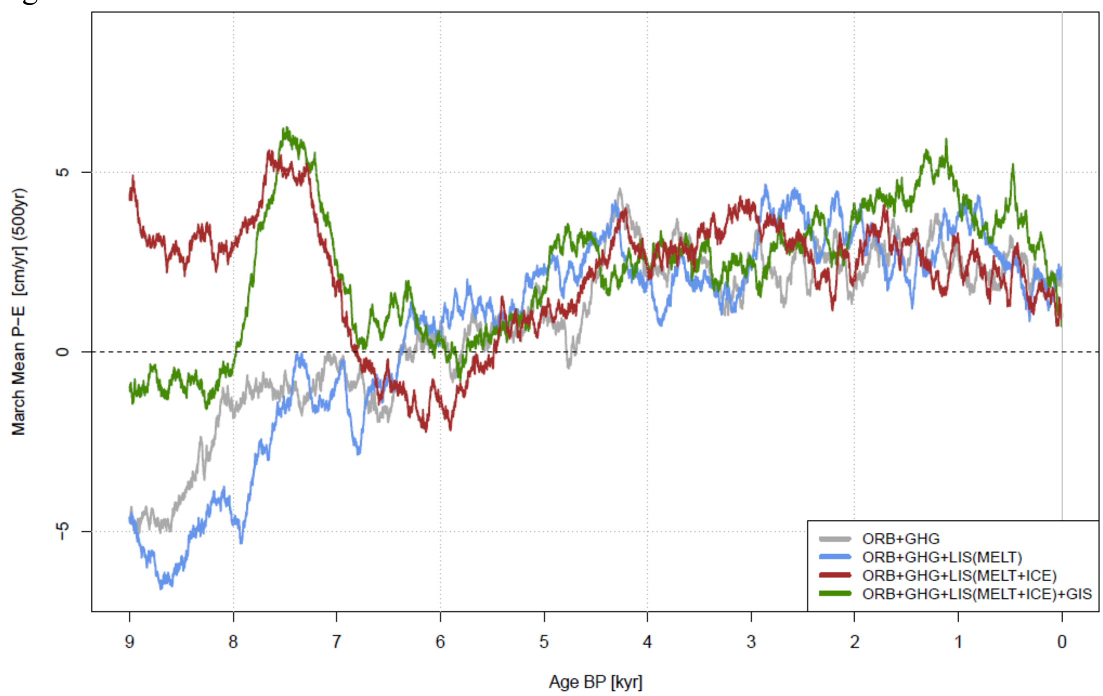

Figure S5.
500-year mean March sea surface salinity (SSS) in the model convection region in the Nordic Seas for the Holocene transient model simulations. The offset in salinity between ORB+GHG and the other experiments is caused by freshwater added from the melting of the LIS (and GIS).

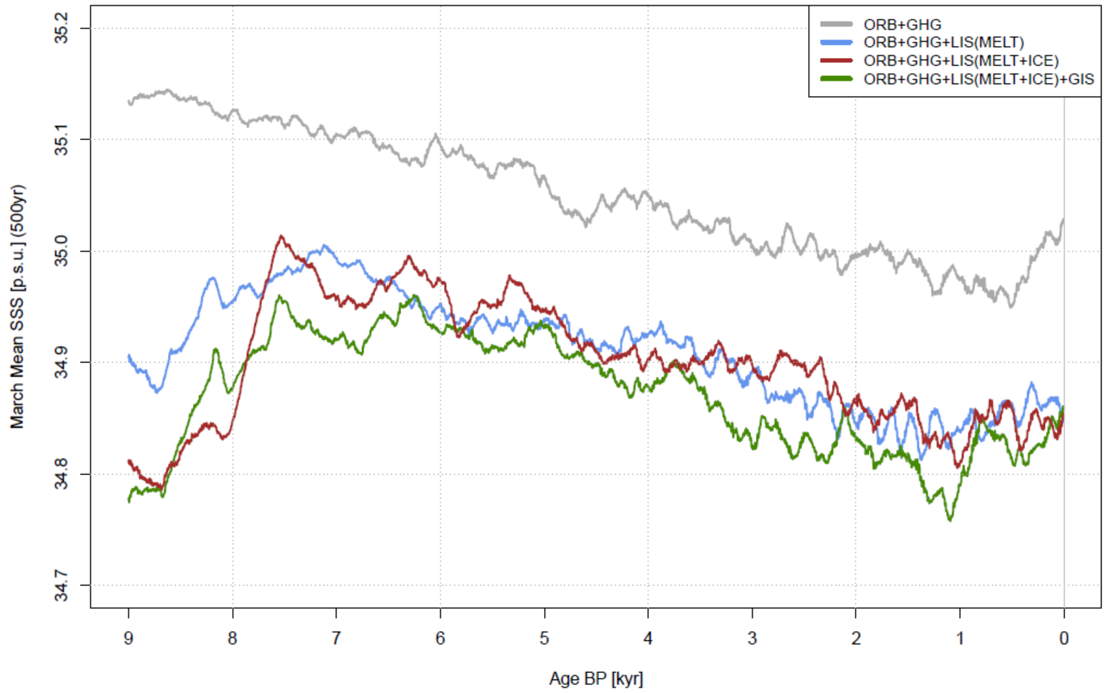

Figure S6.
Predicted 21st century changes in the 50-year mean winter maximum convection layer depth (CLD) in the Nordic Seas region (15-20°E, 76.25-78.75°N), using IPCC emission scenarios B1, A1B and A2 (low to high, respectively). Melting of the GIS was held constant.

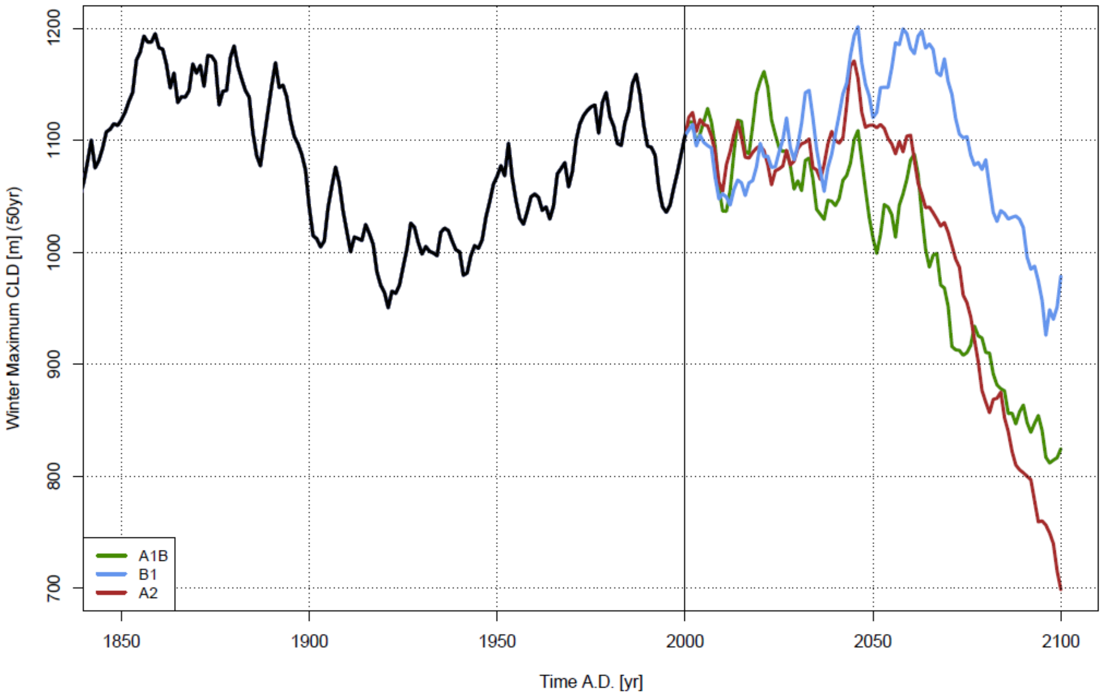

Figure S7.

Predicted 21st century changes in the March SST (15-year mean) in the Nordic Seas convection region using IPCC emission scenarios B1, A1B and A2 (low to high, respectively). Melting of the GIS was held constant.

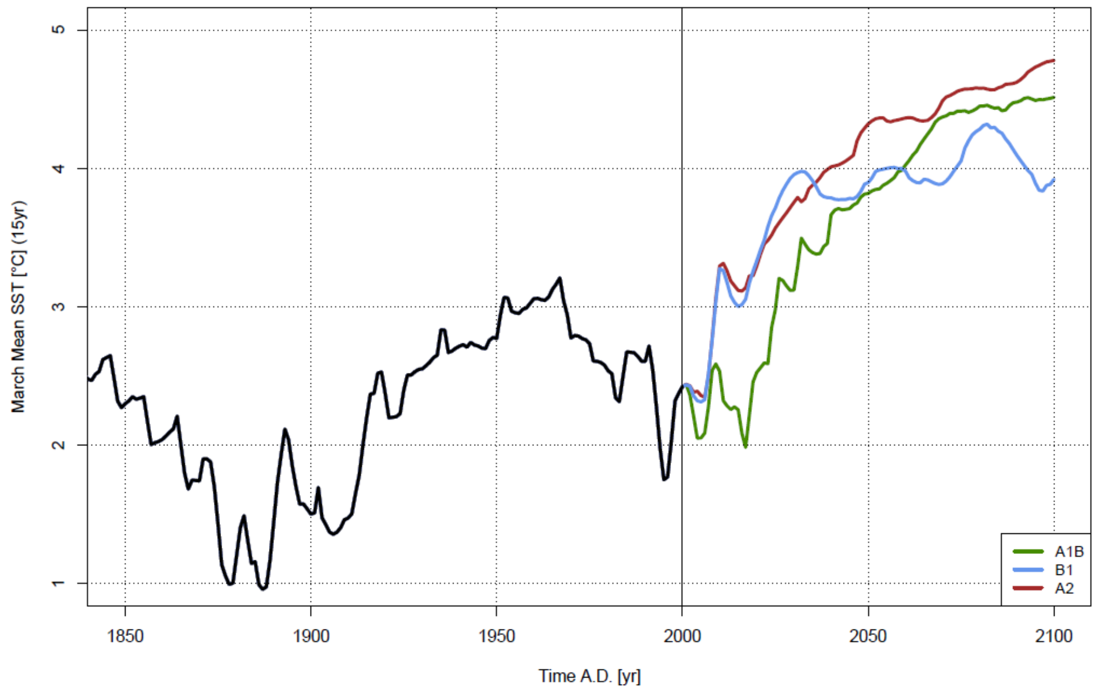

Figure S8.

Predicted 21st century changes in the annual sea-ice flux through Fram Strait (15-year mean) using IPCC emission scenarios B1, A1B and A2 (low to high, respectively). Melting of the GIS was held constant.

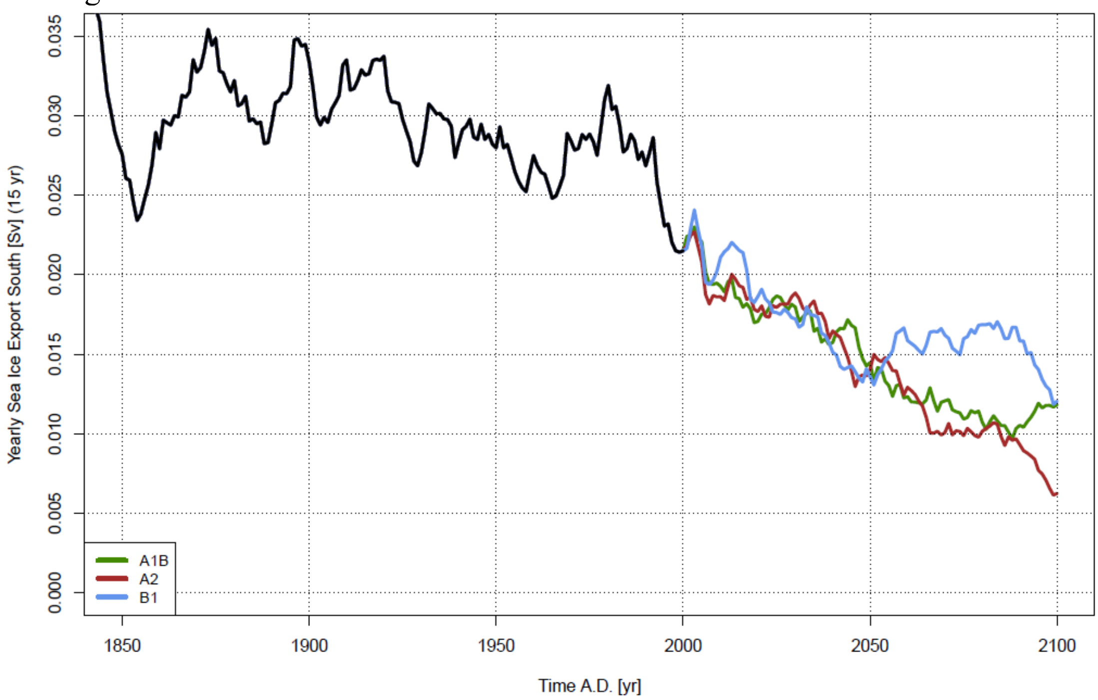

Figure S9.
Predicted 21st century changes in the March precipitation-evaporation balance (15-year mean) in the Nordic Seas convection region using IPCC emission scenarios B1, A1B and A2 (low to high, respectively). Melting of the GIS was held constant.

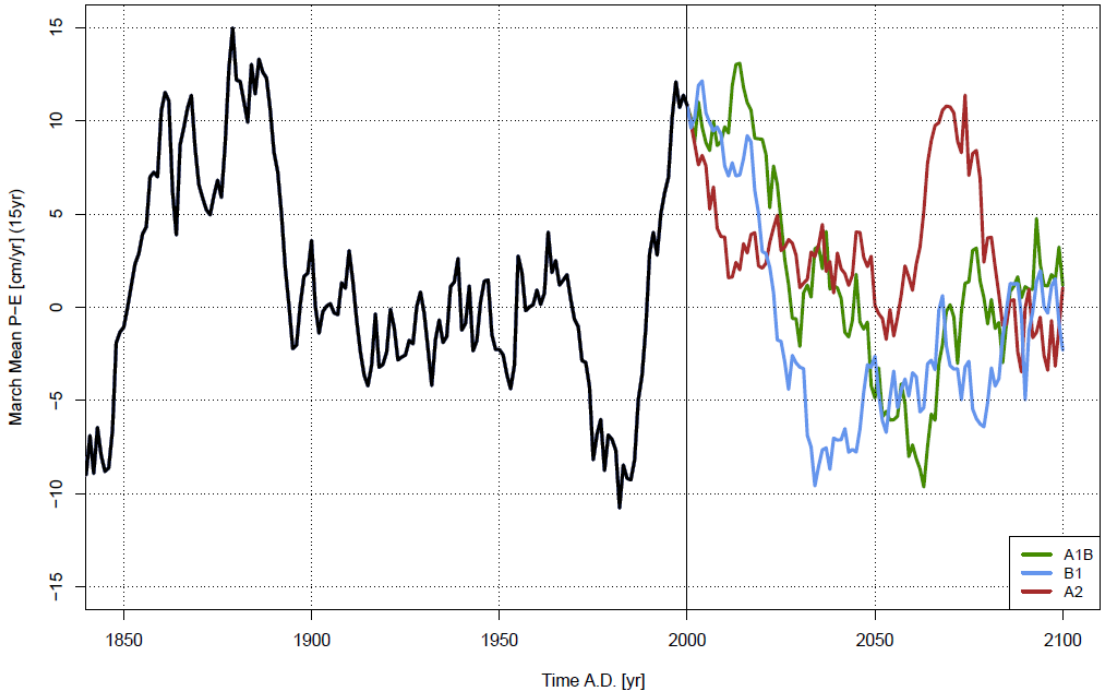

Figure S10.
Predicted 21st century changes in the March SSS (15-year mean) in the Nordic Seas convection region using IPCC emission scenarios B1, A1B and A2 (low to high, respectively). Melting of the GIS was held constant.

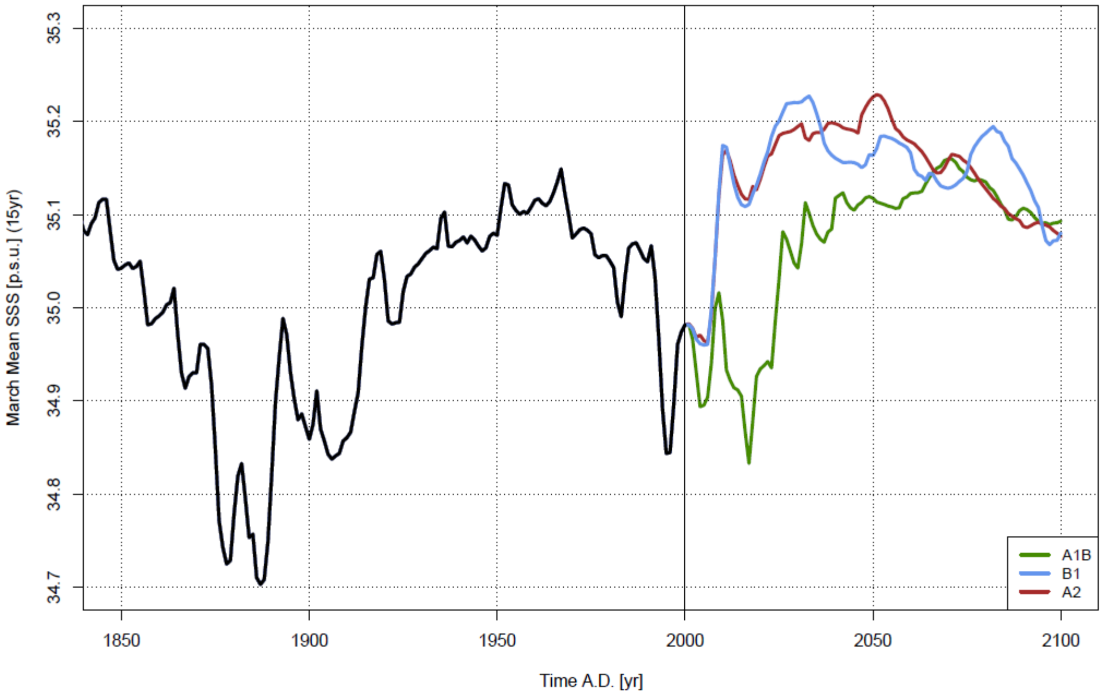

Table S2. Core-site locations

Core	Water depth (m)	Latitude (N)	Longitude (W)
EW9302-30GGC	1188	62° 45.03	20° 40.65
RAPiD-10-1P	1237	62° 58.53	17° 35.37
EW9302-29GGC	1299	62° 36.74	20° 38.25
EW9302-26GGC	1450	62° 19.30	21° 27.44
EW9302-25GGC	1523	62° 03.78	21° 28.33
NEAP-4K	1627	61° 29.91	24° 10.33
EW9302-24GGC	1630	61° 45.77	21° 40.06
ODP 984	1648	61° 26	24° 04
EW9302-23GGC	1695	61° 40.32	21° 43.96
EW9302-22GGC	1800	61° 25.28	21° 53.58
EW9302-11GGC	1977	60° 25.30	23° 23.23
ODP 983	1984	60° 24	23° 38
EW9302-32GGC	2260	61° 20.76	20° 20.93

Table S3. Age models based on linear interpolation between planktic ^{14}C AMS dates. Previously published age model are used for NEAP-4K (Hall et al., 2004), ODP 984 (Praetorius et al., 2008) and RAPiD-10-1P (Thornalley et al., 2010).

Core (EW9302-)	Depth (cm)		ID #	^{14}C Age (years)	Error (years)	Cal. Age (years)
30GGC	0-1	*G. bulloides*	OS-62383	835	35	470
	52-53	*G. bulloides*	OS-62006	7740	40	8190
	80-81	*N. pachyderma (s)*	OS-62000	10650	45	11960
	96	Vedde Ash				12100
29GGC	0-1	*G. bulloides*	OS-16366	905	70	510
	8-9	*G. bulloides*	OS-14207	1020	40	605
	8-9	*N. incompta*	OS-14212	1030	70	
	12-13	*G. bulloides*	OS-19644	1260	35	770
	32-33	*G. bulloides*	OS-14210	1650	40	1230
	32-33	*N. incompta*	OS-14213	1670	35	
	64-65	*G. bulloides*	OS-14211	*3590**	55	
	64-65	*N. incompta*	OS-14218	*3700**	50	
	88-89	*G. bulloides*	OS-41544	3330	40	3200
	112-113	*G. bulloides*	OS-41554	4150	45	4220
	128-129	*G. bulloides*	OS-41545	4610	45	4820
	160-161	*G. bulloides*	OS-41555	5820	45	6260
	184-185	*G. bulloides*	OS-41556	7550	50	7990
	216-217	*G. bulloides*	OS-41557	8950	50	9560
	240-241	*G. bulloides*	OS-14214	9700	50	10390
	248-249	*G. bulloides*	OS-14215	9970	85	10885
	248-249	*N. incompta*	OS-14217	9960	65	10880
	288-289	*N. pachyderma (s)*	OS-14691	10550	55	11840
	288-289	*G. bulloides*	OS-14760	*7729**	100	
	288-289	*N. incompta*	OS-14689	*7740**	55	
	312	Vedde Ash				12100
26GGC	0-1	*G. bulloides*	OS-57709	985	30	555
	60-61	*G. bulloides*	OS-59791	6300	40	6755
	110-111	*G. bulloides*	OS-68074	10050	50	11100
	130	Vedde Ash				12100
	130-131	*N. pachyderma (s)*	OS-59830	10900	90	12400
25GGC	1-2	*G. bulloides*	OS-57650	1180	30	715
	100-101	*G. bulloides*	OS-59832	8620	60	9290

	110	Vedde Ash				12100
	118-119	*N. pachyderma (s)*	OS-68201	11600	55	13000
24GGC	0-1	*G. bulloides*	OS-57647	740	30	410
	120-121	*G. bulloides*	OS-59666	4760	80	5000
	260-261	*G. bulloides*	OS-59669	9210	45	10045
	300-301	*G. bulloides*	OS-57648	10250	45	11220
	320	Vedde Ash				12100
23GGC	0-1	*G. bulloides*	OS-49553	730	30	390
	144-145	*G. bulloides*	OS-59665	3680	40	3600
	200-201	*G. bulloides*	OS-49554	4760	45	5000
	244-245	*G. bulloides*	OS-59671	6500	45	6990
	292-293	*G. bulloides*	OS-60109	8510	45	9000
	336-337	*G. bulloides*	OS-59786	9740	40	10575
	376	Vedde Ash				12100
	388-389	*N. pachyderma (s)*	OS-57646	11550	65	13070
22GGC	0-1	*G. bulloides*	OS-57643	695	35	310
	80-81	*G. bulloides*	OS-57644	2340	40	1950
	324-325	*G. bulloides*	OS-59668	6490	40	6640
	412-413	*G. bulloides*	OS-59787	8260	40	9295
	500-501	*G. bulloides*	OS-57645	10250	45	11220
11GGC	1-2	*G. bulloides*	OS-12985	825	50	460
	40-41	*G. bulloides*	OS-44375	2680	30	2366
	80-81	*G. bulloides*	OS-44376	4030	35	4039
	120-121	*G. bulloides*	OS-44377	5860	30	6277
	160-161	*G. bulloides*	OS-44378	8410	35	9018
	216-217	*G. bulloides*	OS-3692	12300	50	13760
	216-217	*N. pachyderma (s)*	OS-3695	*12850**	80	
32GGC	5-6	*G. bulloides*	OS-57707	505	25	130
	120-121	*G. bulloides*	OS-60553	3860	40	3700
	148-149	*G. bulloides*	OS-60106	4280	35	4400
	200-201	*G. bulloides*	OS-60135	6280	35	6730
	256-257	*G. bulloides*	OS-57708	8110	45	8570

* indicate ^{14}C dates not used in final age models

References

Berger AL (1978) Long-term variations of daily insolation and Quaternary climatic changes. J Atmos Sci 35: 2362-2367

Brovkin, V., Bendtsen, J., Claussen, M., Ganopolski, A., Kubatzki, C., Petoukhov, V., and Andreev, A. (2002) Carbon Cycle, Vegetation, and Climate Dynamics in the Holocene: Experiments with the CLIMBER-2 Model, *Global Biogeochemical Cycles*, 16(4): 1139- doi:10.1029/2001GB001662.

Campin, J.-M., Goosse, H. (1999) Parameterization of density-driven downsloping flow for a coarse-resolution ocean model in zcoordinate. *Tellus A*, 51:412–430

Crowley TJ, Zielinski G, Vinther B, Udisti R, Kreutz K, Cole-Dai J, Castellano E (2008) Volcanism and the Little Ice Age. PAGES News 16: 22-23

Delaygue G, Bard E (2009) Solar forcing based on Be-10 in Antarctica ice over the past millennium and beyond. EGU 2009 General Assembly. #EGU2009-6943

Deleersnijder, E., Beckers, J.M., Campin, J.-M., El Mohajir, M., Fichefet, T., Luyten, P. (1997) Some Mathematical Problems Associated with the Development and use of Marine Models, in: *The Mathematics of Model for Climatology and Environment*, Edited by: Diaz, J. I., NATO ASI Series, Springer-Verlag, I(48), 39-86.

Deleersnijder, E., Campin, J.M. (1995) On the Computation of the Barotropic Mode of a Free-Surface World Ocean Model, *Annales Geophysicae*, 13: 675-688.

Driesschaert, E., Fichefet, T., Goosse, H., Huybrechts, P., Janssens, I., Mouchet, A., Munhoven, G., Brovkin, V., Weber, S. L. (2007) Modeling the influence of Greenland ice sheet melting on the Atlantic meridional overturning circulation during the next millennia, *Geophysical Research Letters*, 34, L10707, doi:10.1029/2007GL029516.

Fichefet, T., Morales Maqueda, M.A. (1997) Sensitivity of a Global Sea Ice Model to the Treatment of Ice Thermodynamics and Dynamics, *Journal of Geophysical Research*, 102(C6): 12609-12646.

Fichefet, T., Morales Maqueda, M.A. (1999) Modelling the Influence of Snow Accumulation and Snow-Ice Formation on the Seasonal Cycle of the Antarctic Sea-Ice Cover, *Climate Dynamics*, 15: 251-268.

Gent, P.R., McWilliams, J.C. (1990) Isopycnal mixing in ocean general circulation models. *Journal of Physical Oceanography* 20:150–155

Goosse, H., Campin, J.M., Fichefet, T., Deleersnijder, E. (1997) Sensitivity of a Global Ice-Ocean Model to the Bering Strait Throughflow, *Climate Dynamics*, 13: 349-358.

Goosse, H., Crowley, T.J., Zorita, E., Ammann, C.M., Renssen, H., Driesschaert, E. (2005) Modelling the climate of the last millennium: What causes the differences between simulations? *Geophysical Research Letters,* 32, L06710, doi:10.1029/2005GL022368.

Goosse, H., Brovkin, V., Fichefet, T., Haarsma, R., Huybrechts, P., Jongma, J., Mouchet, A., Selten, F., Barriat, P-Y., Campin, J-M., Deleersnijder, E., Driesschaert, E., Goelzer, H., Janssens, I., Loutre, M-F., Morales Maqueda, M.A., Opsteegh, T., Mathieu, P-P., Munhoven, G., Pettersson., E.J., Renssen, H., Roche, D.M., Schaeffer, M., Tartinville, B., Timmermann, A., Weber, S.L. (2010) Description of the Earth System Model of Intermediate Complexity LOVECLIM Version 1.2, *Geoscientific Model Development*, 3:603-633 doi: 10.5194/gmd-3-603-2010.

Haarsma, R.J., Selten, F.M., Opsteegh, J.D., Lenderink, G., Liu, Q. (1996) A Coupled Atmosphere Ocean Sea-Ice Model for Climate Predictability Studies, *KNMI, De Bilt,* The Netherlands, 31pp.

Hall, I. R., Bianchi, G. G., and Evans, J. R.: Centennial to millennial scale Holocene climate-deep water linkage in the North Atlantic, Quaternary Science Reviews, 23, 1529-1536, 10.1016/j.quascirev.2004.04.004, 2004.

Hillaire-Marcel, C., de Vernal, A., Bilodeau, G., and Weaver, A. J. (2001) Absence of Deep-Water Formation in the Labrador Sea during the Last Interglacial Period, *Nature*, 410: 1073-1077.

Hillaire-Marcel, C., de Vernal, A., and Piper, D. J. W. (2007) Lake Agassiz Final drainage event in the northwest North Atlantic, *Geophysical Research Letters*, 34: L15601, doi:10.1029/2007GL030396.

IPCC (2000) Special report on emission scenarios. *Cambridge University Press, New York.*

IPCC, 2007: Climate Change 2007: The Physical Science Basis. Contribution of Working Group I to the Fourth Assessment Report of the Intergovernmental Panel on Climate Change [Solomon, S., D. Qin, M. Manning, Z. Chen, M. Marquis, K.B. Averyt, M. Tignor and H.L. Miller (eds.)]. Cambridge University Press, Cambridge, United Kingdom and New York, NY, USA, 996 pp.

Licciardi, J. M., Teller, J. T., and Clark, P. U. (1999) Freshwater routing by the Laurentide Ice Sheet during the last deglaciation, in: Mechanisms of Global Climate Change at Millennial Time Scales, edited by Clark, P., Webb, R., and Keigwin, L., Vol. 112 of *Geophysical Monograph*, pp. 177–201, American Geophysical Union, Washington DC.

Mellor, G.L., Yamada, T. (1982) Development of a turbulence closure model for geophysical fluid problems. *Review of Geophysics and Space Physics* 20:851–875

Opsteegh, J. D., Haarsma, R. J., Selten, F. M., and Kattenberg, A. (1998) ECBILT: A Dynamic Alternative to Mixed Boundary Conditions in Ocean Models, *Tellus A*, 50: 348-367.

Peltier, W. (2004) Global Glacial Isostasy and The Surface Of The Ice-Age Earth: The ICE-5G (VM2) Model and Grace, *Annual Review of Earth and Planetary Sciences*, 32: 111-149.

Pinto JP, Turco RP, Toon OB (1989) Self-limiting physical and chemical effects in volcanic eruption clouds. J Geophys Res 94: 11165-11174. doi:10.1029/JD094iD08p11165

Praetorius, S. K., McManus, J. F., Oppo, D. W., and Curry, W. B.: Episodic reductions in bottom-water currents since the last ice age, Nature Geoscience, 1, 449-452, 10.1038/ngeo227, 2008.

Renssen, H., Seppä, H., Heiri, O., Roche, D.M., Goosse, H., Fichefet, T. (2009) The Spatial and Temporal Complexity of the Holocene Thermal Maximum, *Nature Geoscience*, 2: 411-414.

Roche, D.M., Dokken, T.M., Goosse, H., Renssen, H., Weber, S.L. (2007). Climate of the Last Glacial Maximum: sensitivity studies and model-data comparison with the LOVECLIM coupled model. *Climate of the Past*, 3, 205–224.

Rossow, W.B., Walker, A.W., Beuschel, D.E., Roiter M.D. (1996) International Satellite Cloud Climatology Project (ISCCP) documentation of new cloud datasets, *WMO/TD-No 737I, World Meteorological Organisation*.

Sato M, Hansen JE, McCormick MP, Pollack JB (1993) Stratospheric aerosol optical depths, 1850-1990. J Geophys Res 98: 22987-22994. doi:10.1029/93JD02553

Schmittner, A., Latif, M., Schneider, B. (2005) Model Projections of the North Atlantic Thermohaline Circulation for the 21st Century Assessed by Observations, *Geophysical Research Letters*: 32, L23710, doi:10.1029/2005GL024368.

Thornalley, D. J. R., Elderfield, H., and McCave, I. N.: Intermediate and deep water paleoceanography of the northern North Atlantic over the past 21,000 years, Paleoceanography, 25, 10.1029/2009PA001833, 2010.

Timmreck C, Lorenz SJ, Crowley TJ, Kinne S, Raddatz TJ, Thomas MA, Jungclaus JH (2009) Limited temperature response to the very Large AD 1258 volcanic eruption. Geophys Res Lett 36: L21708. doi:10.1029/2009GL040083

Wang Y-M, Lean JL, Sheeley NR Jr (2005) Modeling the sun's magnetic field and irradiance since 1713. Astrophys J 625: 522-538. doi:10.1086/429689

Wiersma, A. P. and Renssen, H. (2006) Model-data Comparison for the 8.2 ka BP Event: Confirmation of a Forcing Mechanism by Catastrophic Drainage of Laurentide Lakes, *Quaternary Science Reviews*, 25, 63–88, 2006.